Author/s:
Snow, AJD;Sharma, M;Lingford, JP;Zhang, Y;Mui, JWY;Epa, R;Goddard-Borger, ED;Williams, SJ;Davies, GJ

Title:
The sulfoquinovosyl glycerol binding protein SmoF binds and accommodates plant sulfolipids

Date:
2022-01-01

Citation:
Snow, A. J. D., Sharma, M., Lingford, J. P., Zhang, Y., Mui, J. W. Y., Epa, R., Goddard-Borger, E. D., Williams, S. J. & Davies, G. J. (2022). The sulfoquinovosyl glycerol binding protein SmoF binds and accommodates plant sulfolipids. Current Research in Structural Biology, 4, pp.51-58. https://doi.org/10.1016/j.crstbi.2022.03.001.

Persistent Link:
https://hdl.handle.net/11343/306905

Current Research in Structural Biology 4 (2022) 51–58

Contents lists available at ScienceDirect

Current Research in Structural Biology

journal homepage: www.journals.elsevier.com/current-research-in-structural-biology

The sulfoquinovosyl glycerol binding protein SmoF binds and accommodates plant sulfolipids

Alexander J.D. Snow [a], Mahima Sharma [a], James P. Lingford [b,c], Yunyang Zhang [d], Janice W.-Y. Mui [d], Ruwan Epa [d], Ethan D. Goddard-Borger [b,c], Spencer J. Williams [d], Gideon J. Davies [a,*]

[a] York Structural Biology Laboratory, Department of Chemistry, University of York, York, YO10 5DD, UK
[b] The Walter and Eliza Hall Institute of Medical Research, Parkville, Victoria, 3052, Australia
[c] Department of Medical Biology, University of Melbourne, Parkville, Victoria, 3010, Australia
[d] School of Chemistry and Bio21 Molecular Science and Biotechnology Institute, University of Melbourne, Parkville, Victoria, 3010, Australia

ARTICLE INFO

Handling editor: Natalie Strynadka

Keywords:
X-ray crystallography
Substrate-binding protein
Isothermal-titration calorimetry
Sulfoglycolysis

ABSTRACT

Sulfoquinovose (SQ) is the anionic headgroup of the ubiquitous plant sulfolipid, sulfoquinovosyl diacylglycerol (SQDG). SQDG can undergo delipidation to give sulfoquinovosyl glycerol (SQGro) and further glycoside cleavage to give SQ, which can be metabolized through microbial sulfoglycolytic pathways. Exogenous SQDG metabolites are imported into bacteria through membrane spanning transporter proteins. The recently discovered sulfoglycolytic sulfoquinovose monooxygenase (sulfo-SMO) pathway in *Agrobacterium tumefaciens* features a periplasmic sulfoquinovosyl glycerol binding protein, SmoF, and an ATP-binding cassette (ABC) transporter. Here, we use X-ray crystallography, differential scanning fluorimetry and isothermal titration calorimetry to study SQ glycoside recognition by SmoF. This work reveals that in addition to SQGro, SmoF can also bind SQ, a simple methyl glycoside and even a short-chain SQDG analogue. Molecular recognition of these substrates is achieved through conserved interactions with the SQ-headgroup together with more plastic interactions with the aglycones. This suggests that the solute binding protein of *A. tumefaciens,* and related SQ-binding proteins from other sulfoglycolytic pathways, can provide their host organisms direct access to most of the SQ metabolites known to be produced by phototrophs.

1. Introduction

Sulfoquinovose (6-deoxy-6-sulfoglucose, SQ) is a sulfosugar that occurs primarily as the anionic headgroup of the plant sulfolipids collectively termed sulfoquinovosyl diacylglycerol (SQDG) (Benson et al., 1959). SQDG is a constituent of the thylakoid membranes of photosynthetic organisms (Mizusawa and Wada, 2012; Sato et al., 2016) and associates with membrane proteins such as photosystem II (Loll et al., 2005). SQDG is a major global reservoir of organosulfur with an estimated 10 Pg produced annually (Goddard-Borger and Williams, 2017; Harwood and Nicholls, 1979). The catabolism of SQDG occurs in a wide range of gram-positive and gram-negative bacteria through one of five sulfoglycolytic pathways (Snow et al., 2021, J. Liu et al., 2021).

The sulfoglycolytic Embden-Meyerhof-Parnas (sulfo-EMP) (Denger et al., 2012, 2014; Sharma et al., 2021), sulfoglycolytic Entner-Doudoroff (sulfo-ED) (Felux et al. 2015a,b; Li et al., 2020) and sulfoglycolytic sulfofructose transaldolase (sulfo-SFT) (Frommeyer et al., 2020; Y. Liu et al., 2020) pathways involve scission of the six-carbon SQ backbone into two three-carbon fragments: carbons 1–3 are metabolized, while carbons 4–6 are excreted as a three-carbon sulfonate after subsequent reduction to 2,3-dihydroxypropanesulfonate DHPS (by NADH-dependent SLA reductase (YihU) (Sharma et al., 2020)) or oxidation to sulfolactate SL (by NAD^+-dependent SLA dehydrogenase). The sulfoglycolytic transketolase (sulfo-TK pathway) involves stepwise scission of two carbons (carbons 1 and 2, and carbons 3 and 4) from sulfofructose and transfer to G3P, while carbons 5 and 6 form sulfoacetaldehyde, which is reduced and excreted as isethionate (J. Liu et al., 2021). In contrast to all other known pathways, the sulfoglycolytic SQ monooxygenase (sulfo-SMO) pathway involves the cleavage of the sulfur-carbon bond of SQ with excretion of inorganic sulfur (predominantly as sulfite) and enables the utilization of all six carbons of SQ (Sharma et al., 2022, J. Liu et al., 2021). For sulfoglycolytic pathways to catabolise SQ, it must first be

* Corresponding author.
E-mail address: gideon.davies@york.ac.uk (G.J. Davies).

https://doi.org/10.1016/j.crstbi.2022.03.001
Received 11 January 2022; Received in revised form 3 March 2022; Accepted 3 March 2022

liberated from imported SQDG or its delipidated forms sulfoquinovosyl monacylglycerol (SQMG) and sulfoquinovosyl glycerol (SQGro). SQ is hydrolyzed from these molecules by 'gateway' sulfoquinovosidases, which belong to glycoside hydrolase family GH31 (www.cazy.org) (Abayakoon et al., 2018; Speciale et al., 2016), while import of SQ glycosides is mediated by specialized permeases or transport systems.

The sulfo-SMO pathway of *Agrobacterium tumefaciens* utilizes a two-component system, comprised of an $FMNH_2$-dependent SQ monooxygenase and a flavin reductase, to cleave the carbon-sulfur bond of SQ to form 6-oxo-glucose (6-OG) and sulfite (Sharma et al., 2022), (Fig. 1). Reduction of 6-OG to glucose is catalyzed by an NADPH-dependent 6-OG reductase, enabling the product, glucose, to enter central metabolism. The *smo* gene cluster encodes an ATP-binding cassette (ABC) transport system consisting of a pair of identical ATPase domains (SmoE) and two distinct transmembrane domains (SmoG, SmoH). The ABC transporter engages with the periplasmic solute binding protein SmoF, which binds SQGro with sub-micromolar affinity and recruits it for import into the cell (Sharma et al., 2022). The sulfo-ED pathway gene cluster in *Rhizobium leguminosarum* also contains an ABC transporter and putative SQGro binding protein, suggesting that ABC transporters may be utilized in other sulfoglycolytic pathways in different organisms (Li et al., 2020).

Solute binding proteins, such as maltose binding protein (MalE) and SmoF, are associated with ABC transporters and are involved in the recruitment of the substrate ligand to the transmembrane domains to enable ATP-dependent transport across the membrane (Davidson et al., 2008) (Fig. 1). There are seven classes of ABC transporters (Thomas and Tampé, 2020), with the specificity and mechanism of the type 1 ABC transporter maltose transporter $MalEFGK_2$ perhaps the best characterized. Maltose transporter operates in conjunction with a periplasmic substrate binding protein MalE, with maltooligosaccharide loaded-MalE docking with the membrane components $MalFGK_2$ (Quiocho et al., 1997; Spurlino et al., 1991). In free (apo) form MalE adopts an open conformation, and upon ligand binding MalE undergoes a hinge bending motion to a closed conformation. The adoption of the closed conformation is essential for productive interaction of MalE with the cytoplasmic-membrane components of the ABC transporter complex and importation of maltooligosaccharides across the membrane (Duan et al., 2001). The SQ binding protein SmoF, like other solute binding proteins, has a structural fold comprised of two globular lobes (interconnected by polypeptide chains), which undergo conformational changes upon ligand binding (Berntsson et al., 2010; Sharma et al., 2022). Studies of solute binding proteins show that the ligand-free form undergoes equilibration between open and semi-closed states (Tang et al., 2007). In the case of SmoF, once the open ligand-free form binds SQGro (Sharma et al., 2022), it undergoes a domain rotation to a closed conformation that encapsulates the ligand.

Here, we study the ligand specificity of SmoF, showing that in addition to SQGro, it can bind SQ, the simple glycoside SQMe and, unexpectedly, a short-chain derivative of SQDG. The thermodynamic and structural basis of binding for these ligands is explored. This work suggests that SmoF may facilitate the delivery of both SQ, SQGro and even plant sulfolipids to the ABC transporter and that this transporter system allows acquisition of a range of SQ glycosides by the host organism. We

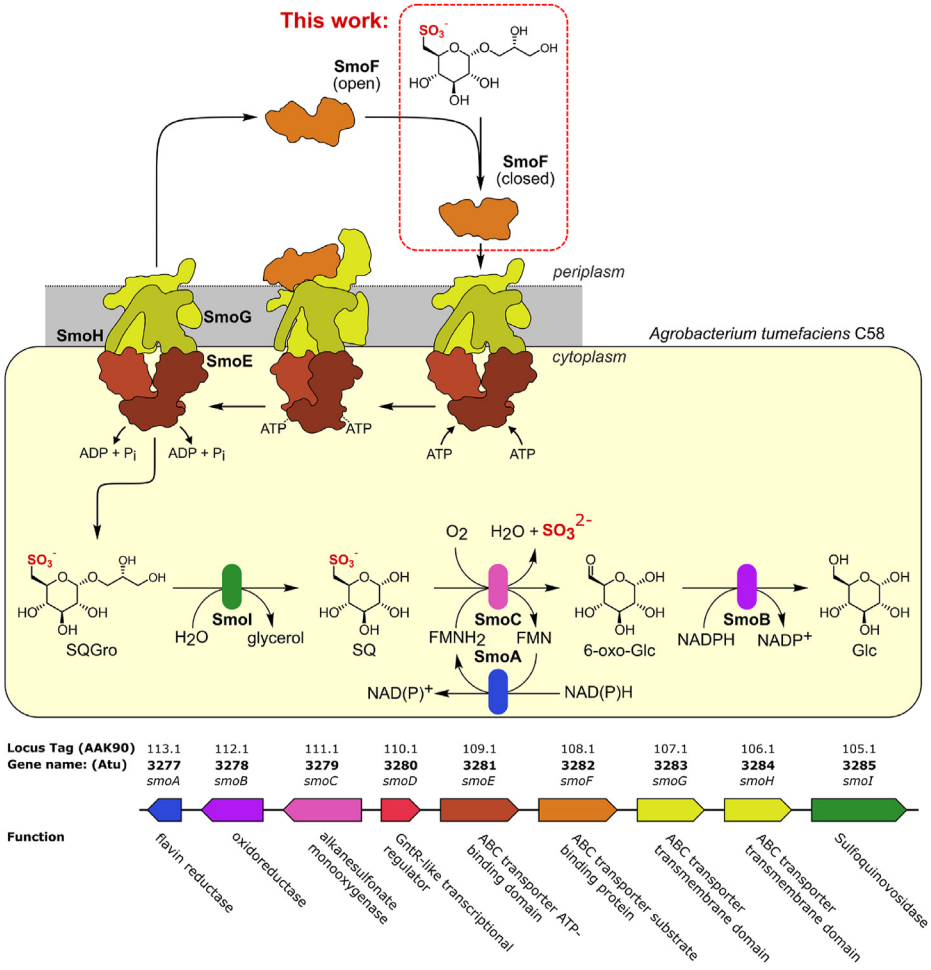

Fig. 1. The sulfoquinovose monooxygenase (sulfo-SMO) pathway of *Agrobacterium tumefaciens*. The SQ-Gro binding protein SmoF works in concert with the ABC transporter SmoE-SmoG-SmoH to transport SQ metabolites into the cytoplasm. SQ glycosides are cleaved by sulfoquinovosidase SmoI, and SQ is converted to glucose and sulfite by $FMNH_2$-dependent monooxygenase SmoC and 6-oxoglucose reductase SmoB.

demonstrate that the residues involved in sulfonate binding are conserved within several other organisms in the taxon *Rhizobiales* but not in putative solute-binding proteins associated with ABC transporters in other sulfoglycolytic bacteria, suggesting that their sulfonate-binding proteins may have evolved other modes of SQ recognition.

2. Materials and methods

2.1. Gene expression and protein purification

Gene expression and purification of SmoF was performed as previously documented (Sharma et al., 2022). Briefly, expression of SmoF was achieved using pET29b(+) vector using BL21(DE3) competent *E. coli*. The native gene sequence for SmoF encodes a signal peptide, but this was deleted for recombinant expression. His6-tagged binding protein was purified by immobilised-metal affinity chromatography (IMAC) on a nickel-nitrilotriacetic acid (NiNTA) column using 50 mM TRIS 300 mM NaCl pH 7.4 containing 30 m M imidazole and the bound protein was eluted using a linear gradient with buffer containing 300 mM imidazole. SmoF fractions were pooled, concentrated and loaded onto a HiLoad 16/600 Superdex 75 gel filtration column pre-equilibrated with 50 mM NaPi, 300 mM NaCl pH 7.4 buffer. The pooled fractions were concentrated to 40 mg/ml for crystallization trials.

2.2. Protein crystallization and optimization

SmoF•SQ crystals were grown in a sitting drop using 20 mg ml^{-1}, in 0.1 M NaBr, NaI, 0.1 M imidazole, MES pH 6.9, 13.5% MPD, PEG 1000, PEG 3350 at 10 °C, with a 5:6 mother liquor: protein ratio. SmoF•SQMe crystals were grown using 50 mg ml^{-1} protein in 0.3 M sodium acetate, 0.1 M BIS-TRIS (pH 5.5) and 35% PEG 2000 MME in a sitting drop, with a 1:1 protein:mother liquor ratio in-drop. In both cases 2 mM ligand was added to protein 10 min prior to drop formation. SmoF•SQDG-(C4:0/C16:0) crystals were grown in sitting drop at 6 °C, with 25 mg ml^{-1} protein and 2.5 mM SQDG-(C4:0/C16:0) dissolved in DMSO, in 25 mM NaPi, 150 mM NaCl pH 7.0, incubated at room temperature with 2.5 mM SQDG-(C4:0/C16:0) for 10 min prior to crystallization. Diffraction quality crystals were collected from a direct scale up of the Morpheus screen (Molecular Dimensions), condition H12. This contains 0.1 M amino acids (0.2M L-Na-glutamate, 0.2 M alanine, 0.2 M glycine, 0.2 M lysine hydrochloride, 0.2 M serine), 0.1 M buffer system 3 pH 8.5 (1 M TRIS, 1 M bicine) and 50% v/v precipitant mix 4 (25% MPD, 25% PEG 1000, 25% PEG 3350). Crystals only formed in premade mother liquor. No cryoprotectant was used on the resultant crystals due to the presence of cryoprotecting PEG solutions in the mother liquor. Crystals were harvested then flash cooled in liquid nitrogen, using nylon CryoLoops (Hampton).

2.3. Data collection and structure determination

All crystals were tested using a Rigaku MicroMax 007HF X-ray generator with an RAXIS IV++ imaging plate detector. Data was collected at 120 K using a 700 Series Cryostream (Oxford Cryosystems). Diffraction pattern quality assessment and resolution estimate performed using ADXV (Porebski et al., 2013). X-ray data collection occurred at the Diamond Light Source, using beamline I-03 during collection mx18598-51. Data collection statistics are available in Table 1. Data indexing and initial processing for SmoF•SQ and SmoF•SQMe was performed at Diamond, using either DIALS or 3dii automated pipelines from the Xia2 package (Beilsten-Edmands et al., 2020; Winter, 2010). For SmoF with SQDG-(C4:0/C16:0), indexing was performed manually using DUI (Beilsten-Edmands et al., 2020). In all cases AIMLESS was used for data reduction and quality assessment (Evans and Murshudov, 2013). Resolution was cut to CC1/2 = 0.5, or to the highest resolution possible while maintaining an outer shell completeness of 80% or higher. Molecular replacement used either MOLREP or PHASER (Vagin and Teplyakov, 2010; McCoy et al., 2007) The model used for the SmoF•SQMe structure was 70FY, and the SmoF•SQMe structure was then used for the other two datasets. Early model building was automated using BUCCANEER (Cowtan, 2006). Model refinement was performed using REFMAC5 employing local NCS restraints in the refinement cycles, and all interactive modelling and validation performed in COOT (Emsley & Cowtan, 2004; Murshudov et al., 2011). All steps excluding manual data integration were performed from within the CCP4i2 system (Potterton et al., 2018). Diagram preparation for molecular models was performed using CCP4MG, Pymol or UCSF Chimera, depending on the desired outcome (McNicholas et al., 2011; Pettersen et al., 2004; Schrödinger, 2015). Analyses of conformational changes and internal cavities were performed using the *DynDom* web server and the CASTp V.3.0 Pymol plugin, respectively (Girdlestone and Hayward, 2016; Tian et al., 2018). We detect anisotropy in SmoF•SQ and SmoF•SQMe datasets as evident from a much higher anisotropic B value for data along the c* axis, affecting the respective data processing statistics. The resolution cut-off for these datasets was chosen based on higher quality of maps and better refinement statistics.

Table 1
Data collection and refinement statistics for SmoF structures complexed with SQ, SQMe, SQDG-(C4:0/C16:0).

	SmoF•SQ	SmoF•SQMe	SmoF•SQDG-(C4:0/C16:0)
Data collection			
Space group	P 3_1 2 1	P 2_1 2_1 2_1	P 2_1
Cell dimensions *a*, *b*, *c* (Å)	102.2, 102.2, 67.96	53.76, 66.27, 99.38	53.22, 69.59, 104.57
α, β, γ (°)	90.0, 90.0, 120.0	90.0, 90.0, 90.0	90.0, 91.54, 90.0
Resolution (Å)	88.5–1.80 (1.84–1.80)	49.6–1.59 (1.62–1.59)	69.6–2.14 (2.20–2.14)
R_{merge}	0.179 (2.77)	0.280 (1.38)	0.093 (0.305)
R_{pim}	0.06 (0.93)	0.148 (0.909)	0.081 (0.265)
$I/\sigma I$	10.1 (1.3)	7.7 (1.3)	8.9 (3.6)
CC1/2	1.0 (0.65)	0.98 (0.68)	0.99 (0.94)
Completeness (%)	100 (100)	99.4 (96.1)	99.9 (100)
Redundancy	19.2 (19.1)	6.9 (5.6)	4.1 (4.1)
Refinement			
Resolution (Å)	1.8	1.59	2.14
No. unique reflections	38847	48233	24477
R_{work}/R_{free}	0.20/0.23	0.24/0.27	0.20/0.26
No. atoms			
Protein	5740	5796	11648
Ligand/ion	27	30	142
Water	138	299	239
B-factors (Å^2)			
Protein	32	20	27
Ligand/ion	23	18	26
Water	34	27	29
R.M.S. deviations			
Bond lengths (Å)	0.0146	0.0143	0.0075
Bond angles (°)	1.85	1.79	1.50
Ramachandran Plot Residues			
In most favourable regions (%)	98.4	98.1	97.8
In allowed regions (%)	1.6	1.6	2.2
Outliers	0.0	0.3	0.0
PDB code	**7YZS**	**7YZU**	**7QHV**

2.4. NanoDSF

NanoDSF was performed in 10 μl sample capillaries on a Prometheus NT.48 (NanoTemper). Excitation was 15% for ligand-free, SQ and SQMe samples, and 20% for SQDG-(C4:0/C16:0) and SQDG-(C18:1/C16:0). The 330/350 nm ratio of fluorescence was recorded between 15 °C and 95 °C, at 1 °C.min^{-1}. Data collection and preliminary analysis performed using ThermalControl (NanoTemper). All SmoF samples were at 1 mg

ml^{-1} in 50 mM Tris, 300 mM NaCl pH 7.5. SQ, SQMe were dissolved in and diluted with ultrapure water with the exception of SQDG analogues (SQDG-(C4:0/C16:0) and SQDG-(C18:1/C16:0)), which were dissolved in DMSO to give a 250 mM stock that was further diluted to final concentration of 2 mM with 50 mM Tris, 300 mM NaCl pH 7.5 for binding studies (with final amount of DMSO co-solvent ranging between 0.4 and 1%). All samples were centrifuged at 13,000 rpm for 5 min prior to loading.

2.5. Isothermal titration calorimetry (ITC)

ITC experiments were performed using a MicroCal iTC200 (GE Healthcare) at 25 °C, with a 750 r.p.m. stirring speed and a reference power of 10 μCal.s^{-1}. SmoF was equilibrated into degassed and filter sterilised ITC buffer (50 mM NaPi, 200 mM NaCl, pH 7.4) by dialysis using 3 kDa MWCO Visking tubing. All ligands were dissolved directly into the same buffer. For SmoF/SQ, 2000 μM SQ was titrated into a cell containing 160 μM SmoF, and for SmoF/SQMe 2000 μM SQMe was titrated into 160 μM SmoF. Both were injected as a series of 15 × 2.94 μl injections with a pre-injection of 1 × 0.4 μl. Delays between injection were set at 120 s, with an initial injection delay of 60 s. All data was processed using PEAQ-ITC (MicroCal).

2.6. Bioinformatics

To find sulfo-SMO and sulfo-ED clusters containing SmoF homologues, the protein sequence of *A. tumefaciens* C58 SmoF was submitted to the NCBI psiBLAST algorithm, searching a non-redundant protein sequence (nr) database. Browsing the outputs allowed identification of homologues in sulfo-SMO and sulfo-ED clusters. To find sulfo-EMP clusters containing SmoF homologues, the *E. coli* sulfoquinovosidase (NP_418314.1, locus tag b3878), SQ mutarotase (NP_418315.3, locus tag b3879), SQ isomerase (NP_418316.4, locus tag b3880), SF kinase (NP_418319.2, locus tag b3883), SFP aldolase (NP_418317.1, locus tag b3881), SLA reductase (NP_418318.1, locus tag b3882) and sulfo-EMP regulator (NP_418320.2, locus tag b3884) were submitted separately as queries to the NCBI BLASTp tool. The database searched was the non-redundant protein sequence (nr) database, with *E. coli* (taxid: 562) sequences excluded. Standard algorithm parameters were used, except the maximum target sequences was set to 10,000. The results were filtered, with only protein sequences with E-value ≤ 5.41e-44 retained. The corresponding nucleotide accession numbers for each protein from all seven searches were extracted, and the seven lists combined and duplicates removed to give a list of candidate genome sequences. This list was converted into a MultiGeneBLAST reference library and searched using the *E. coli* sulfo-EMP gene cluster as a query. Scripts for this pipeline are available on GitHub (https://github.com/jmui-unimelb/Gene-Cluster-Search-Pipeline). Gene clusters possessing a putative SQase, putative SQ isomerase, putative SF kinase and putative SFP aldolase were deemed putative sulfo-EMP operons. These putative sulfo-EMP operons were manually searched to identify their transporter types. Candidate SQBPs were submitted to Clustal 2.1 for multiple sequence alignment, and results were used to generate a cladogram.

3. Results and discussion

The SQ moiety exists in nature as the free sugar SQ, and as glycosides including SQDG and SQGro (Supplementary Fig. S1). To explore the ability of SmoF to bind to different glycosides, we synthesized methyl α-sulfoquinovoside (SQMe), and a naturally occurring SQDG, α-sulfoquinovosyl 1-oleoyl-2-palmitoylglycerol (SQDG-(C18:1/C16:0)) (Zhang et al., 2020). Because the full-length lipids endow this lipoform with poor aqueous solubility we also synthesized a more water-soluble analogue, α-sulfoquinovosyl 1-butanoyl-2-palmitoylglycerol (SQDG-(C4:0/C16:0)), which bears a shorter butanoyl lipid.

Initially, we assessed binding of the analogues to SmoF using nano differential scanning fluorimetry (nanoDSF). NanoDSF uses tryptophan or tyrosine fluorescence to monitor protein unfolding as a function of temperature and allows calculation of a melting temperature (Tm) that describes the thermodynamic stability of the protein or protein-ligand complex. Ligand-free SmoF had Tm of 43.9 °C, which was raised to 54.2 °C in the presence of 2 mM SQ (ΔTm = 10.3 °C). Using 2 mM SQMe gave a Tm of 58.5 °C (ΔTm = 14.6 °C), and in the presence of 2 mM SQDG-(C4:0/C16:0) the Tm of SmoF increased to 51.8 °C (ΔTm = 7.7 °C). In contrast, 2 mM SQDG-(C18:1/C16:0) did not result in a significant change in Tm (Fig. 2c, Supplementary Fig. S2). This may indicate this long-chain SQDG does not bind, that it binds with no change, or may simply reflect the poor solubility of this glycolipid and the formation of micelles unable to bind SQBP (Supplementary Fig. S1). We next studied the direct binding of these ligands to SmoF by isothermal titration calorimetry (ITC). SQ bound with a K_d value of 2.4 μM, and SQMe bound with a K_d value of 11.5 μM, which are 10-fold and 40-fold weaker affinity compared to SQGro, respectively (Fig. 2a and b, Supplementary Fig. S3). ITC was attempted with SQDG-(C4:0/C16:0) but was unsuccessful, possibly due to the formation of lipid micelles leading to phase separation (Fig. 2c; Supplementary Table S1).

Crystals of complexes of SmoF with SQ, SQMe and SQDG-(C4:0/C16:0) were obtained by co-crystallization with SmoF and diffracted to 1.8, 1.59 and 2.14 Å resolution, respectively (Table 1). Crystal structure of SmoF with SQDG-(C4:0/C16:0) was obtained in $P2_1$ space group and contains two copies in the asymmetric unit with no significant differences between the copies. The crystals of SmoF with SQ are in space-group $P3_121$, and SmoF•SQMe was obtained in $P2_12_12_1$, each with one copy in the asymmetric unit. Of the 394 residues present in the protein, 386 were present in the SmoF•SQ structure, 387 in the SmoF•SQMe structure, and 392 in the SmoF•SQDG-(C4:0/C16:0) structure. In all three cases, 95% or more of the amino acids in the protein were observed in the electron density, with exceptions occurring primarily in flexible loops and the affinity tag. In all cases SmoF maintains the globular, primarily α-helical structure with the two-domain fold observed previously (Sharma et al., 2022). Within the SmoF•SQ complex, SQ is present as the α-anomer and adopts a $^4C_1$ (chair) conformation. Its binding interactions involve the C6 sulfonate and sugar C2, C3 and C4 hydroxyls (Fig. 3a). The sulfonate occupies a binding pocket comprised of Gln_{12}-Ser_{43}--Gly_{166}-Thr_{220}. Within this pocket, the side-chain nitrogen of Gln_{12} and side-chain hydroxyl of Thr_{220} engage in a hydrogen bond with one sulfonate oxygen (2.6 Å, 2.9 Å), the second sulfonate oxygen forms a hydrogen bond to the backbone secondary amine of Gly_{166} (2.8 Å), and the third sulfonate oxyanion forms a hydrogen bond to the backbone secondary amide of Ser_{43} (2.9 Å) and an ordered water (3.0 Å). The C1 hydroxyl forms a hydrogen bond with a side-chain secondary amine on His_{13} (2.7 Å). The C2 hydroxyl group forms hydrogen bonds to the side chain carboxyl of Asp_{113} (2.7 Å) and the indole nitrogen of Trp_{276} (2.8 Å). The C3 and C4 hydroxyls each bind one nitrogen of Arg_{345} and the carboxyl oxygen of Asp_{67} (2.9, 2.7, 3.0, 2.5 Å) (Fig. 3a).

The SmoF•SQMe complex contains small differences in binding recognition compared to SQ. The sulfonate pocket is identical with the exception of Gln_{12}, which is too distant (3.6 Å) from the sulfonate oxygen to form a hydrogen bond. His_{13}, which is on the same loop, is unable to form a hydrogen bond with the C1 oxygen as it is now present as a glycoside in SQMe. All other interactions are identical to those observed with SQ (Fig. 3b). The SmoF•SQDG-(C4:0/C16:0) complex involves identical interactions as for SQMe with the C2-4 hydroxyl groups, and within the sulfonate binding pocket. The palmitic acid chain protrudes through the top of the binding pocket and forms a crystal contact with another SmoF molecule in the asymmetric unit (Supplementary Fig. S4).

SQ and SQMe reside within an internal cavity that entirely encloses the ligand (Fig. 3d and e). For SQ the volume is 297 $Å^3$ and for SQMe is 447 $Å^3$, 66% larger. The cavity for SQGro is 476 $Å^3$, 6% larger than SQMe (Supplementary Fig. S5). As noted above, SQDG-(C4:0/C16:0) is not fully enclosed by the protein and the cavity features three openings. One of these is occupied by the protruding palmitoyl chain, while the other two

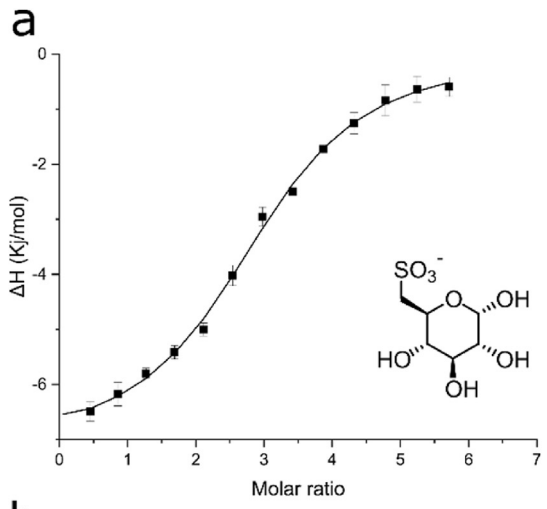

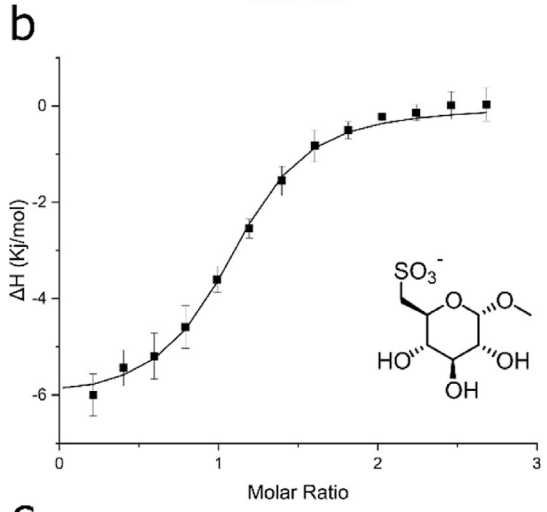

c

Condition	Tm (°C)	Tm shift (°C)	K_D (μM)
Ligand-free	43.9±0.1	-	-
SQGro	59.2±0.8	15.3	0.29±0.17
SQ	54.2±0.8	10.3	8.65±2.4
SQMe	58.3±2.0	14.4	11.5±2.3
SQDG (C4:0/C16:0)	51.8±0.8	7.9	-
SQDG (C18:1/C16:0)	42.9±0.2	-1.0	-

Fig. 2. Binding affinity of SQ and its glycosides for SmoF. a) Isothermal titration calorimogram showing titration of SQ into SmoF. b) Calorimogram of SQMe into SmoF. c) Melting temperature (T_m) of SmoF, as determined by differential scanning fluorimetry, the T_m shift relative to apo-SmoF, and K_d values determined by ITC for SQ, SQMe, SQDG-(C4:0/C16:0) and SQDG-(C18:1/C16:0). Dissociation constants for SQDG-(C4:0/C16:0) and SQDG-(C18:1/C16:0) could not be measured (noted by a dash). Data for SQGro (in blue) was reported in (Sharma et al., 2022) and has been included for comparison. (For interpretation of the references to colour in this figure legend, the reader is referred to the Web version of this article.)

are near the sulfonate. The internal volume of the cavity at 1283 Å^3 is > 4 times larger than that of the SmoF•SQ complex, with a large non-polar region occupied by the butanoyl chain of SQDG-(C4:0/C16:0) (Fig. 3f and g).

The structures of the SmoF complexes with SQ, SQMe and SQDG-(C4:0/C16:0) show large conformational changes relative to the ligand-free form, as observed previously with SQGro (Sharma et al., 2022), and undergo interdomain rotations of up to 33° compared to the unliganded state (Fig. 3g). This movement centers around a pair of hinges, which are found in other SBPs. MalE features a comparable closure angle upon ligand binding (37°) (Tang et al., 2007) (Supplementary Fig. S6). In the SmoF•SQDG-(C4:0/C16:0) complex, ligand binding is accompanied by an upwards deflection in α-helix 1 by 9.8 Å. This moves Gln_{12} and His_{13} away from SQDG-(C4:0/C16:0) allowing its large lipid groups to bind (Supplementary Figs. S7 and S8). Collectively, this data shows that SmoF retains its interactions around the sulfosugar yet has sufficient conformational plasticity to accommodate larger aglycones. For the diacyl glycerol substituent this enables binding even though the entire lipid chain cannot be contained within the binding pocket.

The ligand complexes described above identify a set of residues that are involved in binding a range of SQ analogues, and thus could potentially serve to identify SQ-binding proteins. Previous work has identified several other sulfoglycolytic clusters containing likely SQ-binding proteins in association with ABC transporters: the sulfo-ED gene cluster of *R. leguminosarum* SRDI565 contains a SmoF homologue with 80% sequence identity (Li et al., 2020), and a SmoF homologue was identified in the SMO gene cluster of *Rhizobium oryzae* with 78% identity (Sharma et al., 2022). To identify other candidate SQ-binding proteins, we performed a search for sulfoglycolytic operons that contained putative SQ binding proteins and ABC cassettes. We identified a candidate sulfo-SMO gene cluster in *Neorhizobium galagae* str. DS1499; a candidate sulfo-ED gene cluster in *Microlunatus phosphovorus* NM-1; and candidate sulfo-EMP gene clusters in *Vibrio barjaei* str. 3062 and *Tetrasphaera* sp. Soil756, all of which contained genes encoding SmoF homologues and ABC transporters (Fig. 4a). Sulfo-TK clusters containing a putative SQ binding protein and ABC cassette were reported by Liu and co-workers (Liu et al., 2021). A cladogram of these putative SQ binding proteins shows close homology between the proteins in *Rhizobiales* but otherwise no relationship between sequence identity and the sulfoglycolysis pathway (Fig. 4b).

We next studied whether sulfonate binding pockets were conserved across SmoF homologues as well as other sulfonate-targeting solute binding proteins. Thus, we included SsuA from *E. coli* and *Xanthomonas citri* (Beale et al., 2010; Tófoli De Araújo et al., 2013) and the taurine-binding protein TauA from *E. coli* (Qu et al., 2019), which are solute-binding proteins associated with ABC transporters that bind assorted alkanesulfonates. We also included MalE as a well-characterized SBP that binds a non-sulfonated ligand. Multiple sequence alignment of the SmoF homologues, SsuA, TauA and MalE revealed conservation of the *A. tumefaciens* SmoF sulfonate binding pocket with only *R. leguminosarum* and *R. oryzae* putative SQ-binding proteins (Supplementary Fig. S9). The SQ hydroxyl-binding arginine and aspartic acid residues are conserved in *Neorhizobium* but not among other putative SQ-binding proteins. The poor conservation of binding residues across putative SQ-binding proteins stands in contrast to the strongly conserved sulfonate binding residues present in SQases (Abayakoon et al., 2018; Speciale et al., 2016), which have been used to identify new sulfoglycolysis gene clusters (Liu et al., 2021). There was no conservation of sulfonate binding residues in SsuA or TauA, or in MalE.

4. Conclusions and future work

We show that the solute binding protein SmoF can bind SQ and SQMe, in addition to SQGro as previously reported (Sharma et al., 2022). The protein-ligand interactions are almost identical in all cases, and these ligands result in a large conformational change in the protein versus the apo form, and complete enclosure of the ligand. We also show that SmoF can bind a simplified SQDG. Despite the large lipid groups, binding occurs through largely conserved interactions with the SQ headgroup but involves plasticity in its binding site to partially accommodate the lipid groups. Minor conformational changes in the protein result in an opening from which the lipids protrude. These results suggest that SmoF may

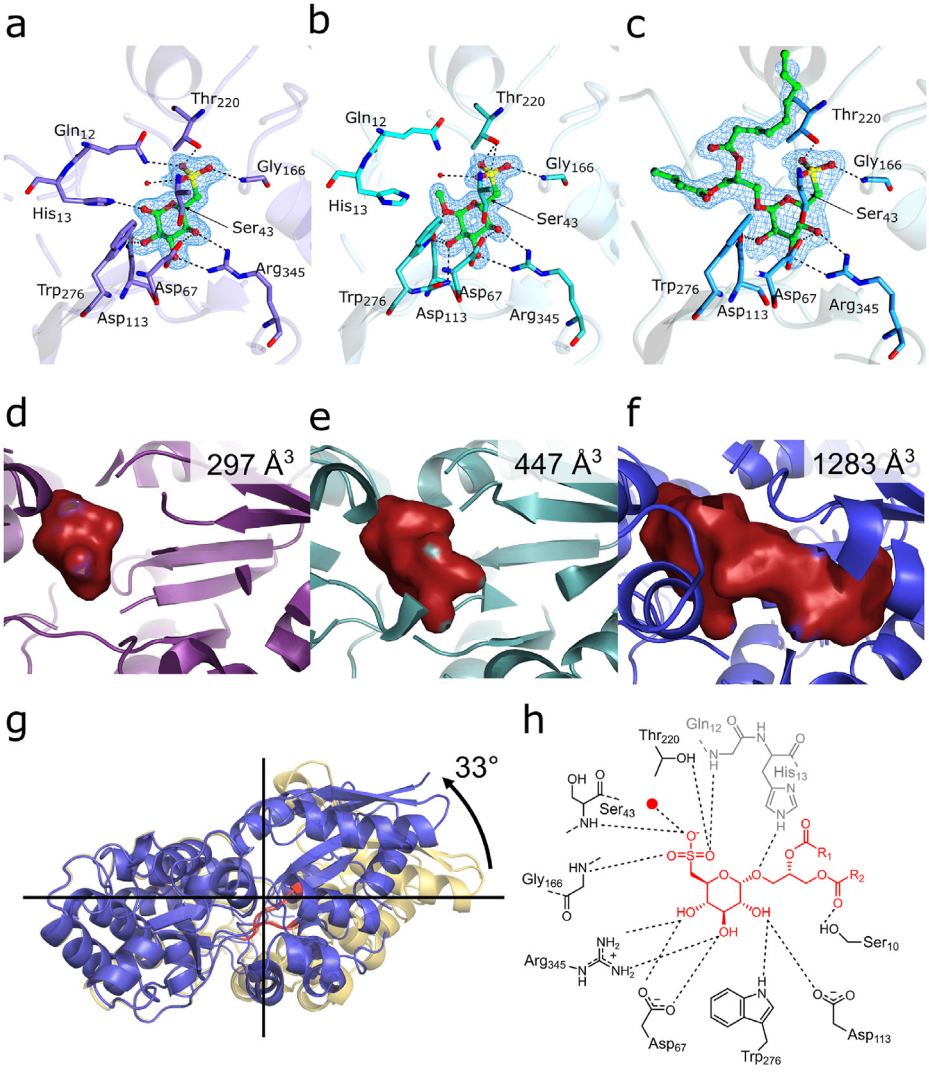

Fig. 3. Structural basis and induced conformational changes for binding of SQ and its derivatives to SmoF. SmoF-ligand complex formation with a) SQ, b) SQMe, and c) SQDG-(C4:0/C16:0). d-f) Internal cavities filled by SQ, SQMe and SQDG-(C4:0/C16:0), as detected using the CASTp server. g) Superposition of ligand-free SmoF (yellow) and complex with SQDG-(C4:0/C16:0) (blue). Hinge angle and domain selection performed using the DynDom web server, and hinge residues highlighted in red. h) Binding interactions of SQ and glycosides. Interactions present in SQ complex but not SQMe or SQDG-(C4:0/C16:0) in grey. In all cases electron density (2Fo-Fc) has been contoured to 1.0 σ or 0.44 e/Å^3 for SmoF•SQ, 0.61 e/Å^3 for SmoF•SQMe and 0.44 e/Å^3 for SmoF•SQDG-(C16:0/C4:0). (For interpretation of the references to colour in this figure legend, the reader is referred to the Web version of this article.)

allow capture of free SQ, SQGro and even lipidated SQ glycosides such as SQMG and SQDG, allowing metabolism of the lipidic part in addition to the SQ and the glycerol. Previously, there has been no evidence that SQDG can be completely metabolized by sulfoglycolytic organisms. Instead, various non-specific lipases have been reported that can cleave the lipid chains (Snow et al., 2021), suggesting that the sulfo-SMO pathway is used in partnership with non-sulfoglycolytic organisms (possibly including plants) that excise and metabolize the energy-rich lipid chains of SQDG, releasing the sulfosugar SQGro. However, the ability of SmoF to bind SQDG suggests that *A. tumefaciens* can on its own achieve the import of SQDG and SQMG. Within this scenario, SmoF, working in concert with *A. tumefaciens* sulfoquinovosidase SmoI, which is expressed with a signal peptide that will direct expression to the periplasm, enables capture of the full carbon-content of SQDG/SQMG. Possibly, this could allow *A. tumefaciens* to utilize intact sulfolipids as a nutrient upon infecting a plant host.

A search for other ABC transporters and associated solute binding proteins in sulfoglycolytic gene clusters led to identification of ABC transporter systems similar to that of *A. tumefaciens* in organisms with gene clusters encoding sulfo-SMO, sulfo-ED, sulfo-EMP, sulfo-SFT and sulfo-TK pathways. This complements earlier reports showing that sulfo-EMP and sulfo-ED (Denger et al., 2014; Felux et al. 2015a,b) gene clusters also contained TauE transporters of the 4-toluene sulfonate uptake permease (TSUP) family (Shlykov et al., 2012) to import SQ and its glycosides. The occurrence of TSUP family or ABC transporter systems in various sulfoglycolysis gene clusters suggests that the specific transporter used to import the sulfosugar substrate is not restricted to a particular pathway. Sequence alignment of putative SQ-binding proteins from this range of organisms revealed that SQ binding residues identified in *A. tumefaciens* SmoF are not well conserved, and thus that acquisition of SQ-binding function may have arisen through independent evolutionary events. Thus, sequence-based searches for new SQ-binding proteins may have poor predictive power, and will require consideration of genetic context and whether the solute binding protein and ABC transporter are associated with a sulfoglycolytic gene cluster. Finally, the ability of SmoF to bind SQ glycosides bearing extended lipid chains means it may be possible to exploit this SQ-binding protein to bind to SQ-linked structures for affinity-based protein capture and purification applications, in a way analogous to the use of maltose-binding protein that binds its cognate ligands (K_d = 0.5–2 μm) with similar affinities.

Funding

GJD is supported by the Royal Society Ken Murray Research Professorship. MS and AS were funded by the Leverhulme Trust (grant RPG-2017-190) and MS subsequently by the Biotechnology and Biological Sciences Research Council (BB/W003805/1). SJW is supported by the Australian Research Council (DP180101957 and DP210100233). EDGB is supported by the Brian M. Davis Charitable Foundation Centenary Fellowship, National Health and Medical Research Council of Australia

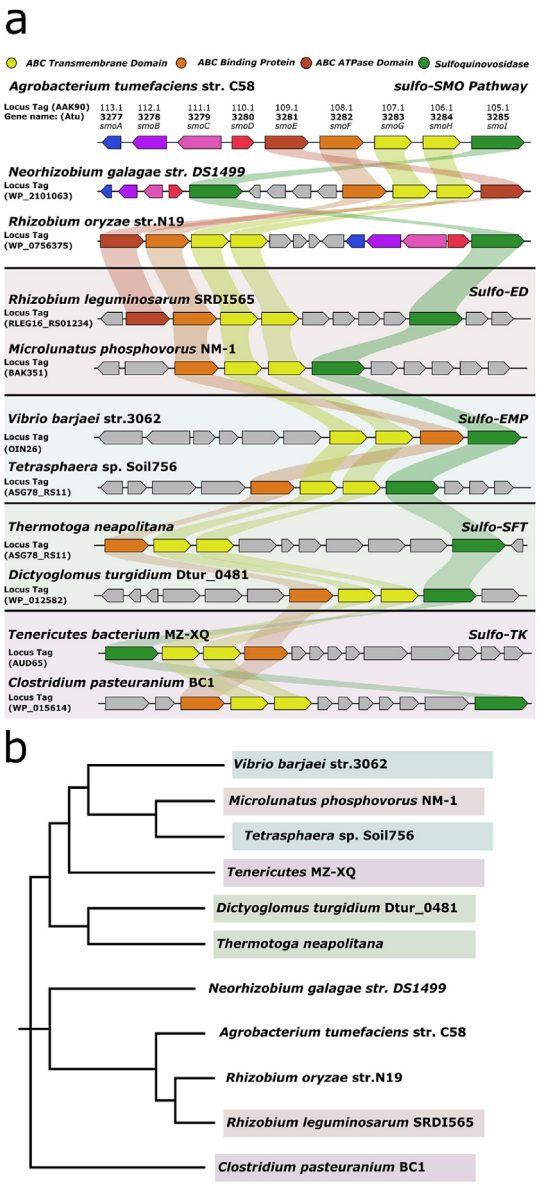

Fig. 4. Comparison of *A. tumefaciens* sulfo-SMO gene cluster with other proposed sulfoglycolytic gene clusters containing SmoF homologues. a) Gene clusters for sulfoglycolytic sulfo-SMO, sulfo-ED, sulfo-EMP, sulfo-TAL and sulfo-TK pathways containing ABC transporters featuring a sulfoquinovose binding protein. b) Cladogram of SmoF and homologues found in different organisms featuring sulfoglycolysis pathways in their core genome.

(NHMRC) project grants GNT1139546, GNT1139549and GNT2000517, and acknowledges support from The Walter and Eliza Hall Institute of Medical Research, the Australian Cancer Research Fund and a Victorian State Government Operational Infrastructure support grant.

CRediT authorship contribution statement

Alexander J.D. Snow: Methodology, Investigation. **Mahima Sharma:** Methodology, Investigation. **Yunyang Zhang:** Methodology, Investigation. **Janice W.-Y. Mui:** Methodology, Investigation. **Ruwan Epa:** Methodology, Investigation. **Ethan D. Goddard-Borger:** Conceptualization, Project administration, Supervision, Funding acquisition. **Spencer J. Williams:** Conceptualization, Project administration, Supervision, Funding acquisition. **Gideon J. Davies:** Conceptualization, Project administration, Supervision, Funding acquisition.

Declaration of competing interest

The authors declare that they have no known competing financial interests or personal relationships that could have appeared to influence the work reported in this paper.

Acknowledgements

We thank Dr. Johan Turkenburg and Sam Hart from maintaining X-ray data collection facilities in York and coordinating Diamond data collection, whose staff are also thanked for provision of beamline facilities (project mx18598). We also thank Prof. Eleanor Dodson FRS for helpful discussions.

Appendix A. Supplementary data

Supplementary data to this article can be found online at https://doi.org/10.1016/j.crstbi.2022.03.001.

References

Abayakoon, P., Jin, Y., Lingford, J.P., Petricevic, M., John, A., Ryan, E., Wai-Ying Mui, J., Pires, D.E.V., Ascher, D.B., Davies, G.J., Goddard-Borger, E.D., Williams, S.J., 2018. Structural and biochemical insights into the function and evolution of sulfoquinovosidases. ACS Cent. Sci. 4, 1266–1273. https://doi.org/10.1021/acscentsci.8b00453.

Beale, J., Lee, S.Y., Iwata, S., Beis, K., 2010. Structure of the aliphatic sulfonate-binding protein SsuA from Escherichia coli. Acta Crystallogr. Sect. F Struct. Biol. Cryst. Commun. 66, 391–396. https://doi.org/10.1107/S1744309110006226.

Beilsten-Edmands, J., Winter, G., Gildea, R., Parkhurst, J., Waterman, D., Evans, G., 2020. Scaling diffraction data in the DIALS software package: algorithms and new approaches for multi-crystal scaling. Acta Crystallogr. Sect. D Struct. Biol. 76, 385–399. https://doi.org/10.1107/S2059798320003198.

Benson, A.A., Daniel, H., Wiser, R., 1959. A sulfolipid IN plants. Proc. Natl. Acad. Sci. Unit. States Am. 45, 1582–1587. https://doi.org/10.1073/pnas.45.11.1582.

Berntsson, R.P.A., Smits, S.H.J., Schmitt, L., Slotboom, D.J., Poolman, B., 2010. A structural classification of substrate-binding proteins. FEBS Lett. 584, 2606–2617. https://doi.org/10.1016/j.febslet.2010.04.043.

Cowtan, K., 2006. The Buccaneer software for automated model building. 1. Tracing protein chains. Acta Crystallogr. Sect. D Biol. Crystallogr. 62, 1002–1011. https://doi.org/10.1107/S0907444906022116.

Davidson, A.L., Dassa, E., Orelle, C., Chen, J., 2008. Structure, function, and evolution of bacterial ATP-binding cassette systems. Microbiol. Mol. Biol. Rev. 72, 317–364. https://doi.org/10.1128/mmbr.00031-07.

Denger, K., Huhn, T., Hollemeyer, K., Schleheck, D., Cook, A.M., 2012. Sulfoquinovose degraded by pure cultures of bacteria with release of C3-organosulfonates: complete degradation in two-member communities. FEMS Microbiol. Lett. 328, 39–45. https://doi.org/10.1111/j.1574-6968.2011.02477.x.

Denger, K., Weiss, M., Felux, A.K., Schneider, A., Mayer, C., Spiteller, D., Huhn, T., Cook, A.M., Schleheck, D., 2014. Sulphoglycolysis in Escherichia coli K-12 closes a gap in the biogeochemical sulphur cycle. Nature 507, 114–117. https://doi.org/10.1038/nature12947.

Duan, X., Hall, J.A., Nikaido, H., Quiocho, F.A., 2001. Crystal structures of the maltodextrin/maltose-binding protein complexed with reduced oligosaccharides: flexibility of tertiary structure and ligand binding. J. Mol. Biol. 306, 1115–1126. https://doi.org/10.1006/jmbi.2001.4456.

Evans, P.R., Murshudov, G.N., 2013. How good are my data and what is the resolution? Acta Crystallogr. Sect. D Biol. Crystallogr. 69, 1204–1214. https://doi.org/10.1107/S0907444913000061.

Felux, A.K., Franchini, P., Schleheck, D., 2015a. Permanent draft genome sequence of sulfoquinovose-degrading Pseudomonas putida strain SQ1. Stand. Genomic Sci. 10, 1–6. https://doi.org/10.1186/s40793-015-0033-x.

Felux, A.K., Spiteller, D., Klebensberger, J., Schleheck, D., 2015b. Entner-Doudoroff pathway for sulfoquinovose degradation in Pseudomonas putida SQ1. Proc. Natl. Acad. Sci. U.S.A. 112, E4298–E4305. https://doi.org/10.1073/pnas.1507049112.

Frommeyer, B., Fiedler, A.W., Oehler, S.R., Hanson, B.T., Loy, A., Franchini, P., Spiteller, D., Schleheck, D., Hanson, S.R., Loy, B.T., 2020. Environmental and intestinal phylum Firmicutes bacteria metabolize the plant sugar sulfoquinovose via a 6-deoxy-6-sulfofructose transaldolase pathway. iScience 23, 101510. https://doi.org/10.1016/j.isci.2020.101510.

Girdlestone, C., Hayward, S., 2016. The DynDom3D webserver for the analysis of domain movements in multimeric proteins. J. Comput. Biol. 23, 21–26. https://doi.org/10.1089/cmb.2015.0143.

Goddard-Borger, E.D., Williams, S.J., 2017. Sulfoquinovose in the biosphere: occurrence, metabolism and functions. Biochem. J. 474, 827–849. https://doi.org/10.1042/BCJ20160508.

Harwood, J.L., Nicholls, R.G., 1979. The plant sulpholipid– a major component of the sulphur cycle. Biochem. Soc. Trans. 7, 440–447. https://doi.org/10.1042/bst0070440.

Li, J., Epa, R., Scott, N.E., Skoneczny, D., Sharma, M., Snow, A.J.D., Lingford, J.P., Goddard-Borger, E.D., Davies, G.J., Mcconville, M.J., Williams, S.J., 2020. A sulfoglycolytic entner-doudoroff pathway in rhizobium leguminosarum bv. trifolii SRDI565. Appl. Environ. Microbiol. 86. https://doi.org/10.1128/AEM.00750-20.

Liu, J., Wei, Y., Ma, K., An, J., Liu, X., Liu, Y., Ang, E.L., Zhao, H., Zhang, Y., 2021. Mechanistically diverse pathways for sulfoquinovose degradation in bacteria. ACS Catal. 11, 14740–14750. https://doi.org/10.1021/acscatal.1c04321.

Liu, Y., Wei, Y., Zhou, Y., Ang, E.L., Zhao, H., Zhang, Y., 2020. A transaldolase-dependent sulfoglycolysis pathway in Bacillus megaterium DSM 1804. Biochem. Biophys. Res. Commun. 533, 1109–1114. https://doi.org/10.1016/j.bbrc.2020.09.124.

Loll, B., Kern, J., Saenger, W., Zouni, A., Biesiadka, J., 2005. Towards complete cofactor arrangement in the 3.0 Å resolution structure of photosystem II. Nature 438, 1040–1044. https://doi.org/10.1038/nature04224.

McCoy, A.J., Grosse-Kunstleve, R.W., Adams, P.D., Winn, M.D., Storoni, L.C., Read, R.J., 2007. Phaser crystallographic software. J. Appl. Crystallogr. 40 (4), 658–674. https://doi.org/10.1107/S0021889807021206.

McNicholas, S., Potterton, E., Wilson, K.S., Noble, M.E.M., 2011. Presenting your structures: the CCP4mg molecular-graphics software. Acta Crystallogr. Sect. D Biol. Crystallogr. 67, 386–394. https://doi.org/10.1107/S0907444911007281.

Mizusawa, N., Wada, H., 2012. The role of lipids in photosystem II. Biochim. Biophys. Acta Bioenerg. https://doi.org/10.1016/j.bbabio.2011.04.008.

Murshudov, G.N., Skubák, P., Lebedev, A.A., Pannu, N.S., Steiner, R.A., Nicholls, R.A., Winn, M.D., Long, F., Vagin, A.A., 2011. REFMAC5 for the refinement of macromolecular crystal structures. Acta Crystallogr. Sect. D Biol. Crystallogr. 67, 355–367. https://doi.org/10.1107/S0907444911001314.

Pettersen, E.F., Goddard, T.D., Huang, C.C., Couch, G.S., Greenblatt, D.M., Meng, E.C., Ferrin, T.E., 2004. UCSF Chimera - a visualization system for exploratory research and analysis. J. Comput. Chem. 25, 1605–1612. https://doi.org/10.1002/jcc.20084.

Porebski, B.T., Ho, B.K., Buckle, A.M., 2013. Interactive visualization tools for the structural biologist. J. Appl. Crystallogr. 46, 1518–1520. https://doi.org/10.1107/S0021889813017858.

Potterton, L., Agirre, J., Ballard, C., Cowtan, K., Dodson, E., Evans, P.R., Jenkins, H.T., Keegan, R., Krissinel, E., Stevenson, K., Lebedev, A., McNicholas, S.J., Nicholls, R.A., Noble, M., Pannu, N.S., Roth, C., Sheldrick, G., Skubak, P., Turkenburg, J., Uski, V., Von Delft, F., Waterman, D., Wilson, K., Winn, M., Wojdyr, M., 2018. CCP 4 i 2: the new graphical user interface to the CCP 4 program suite. Acta Crystallogr. Sect. D Struct. Biol. 74, 68–84. https://doi.org/10.1107/S2059798317016035.

Qu, F., ElOmari, K., Wagner, A., De Simone, A., Beis, K., 2019. Desolvation of the substrate-binding protein TauA dictates ligand specificity for the alkanesulfonate ABC importer TauABC. Biochem. J. 476, 3649–3660. https://doi.org/10.1042/BCJ20190779.

Quiocho, F.A., Spurlino, J.C., Rodseth, L.E., 1997. Extensive features of tight oligosaccharide binding revealed in high-resolution structures of the maltodextrin transport/chemosensory receptor. Structure 5, 997–1015. https://doi.org/10.1016/S0969-2126(97)00253-0.

Sato, N., Kobayashi, S., Aoki, M., Umemura, T., Kobayashi, I., Tsuzuki, M., 2016. Identification of genes for sulfolipid synthesis in primitive red alga Cyanidioschyzon merolae. Biochem. Biophys. Res. Commun. 470, 123–129. https://doi.org/10.1016/j.bbrc.2016.01.006.

Schrödinger, L., 2015. The PyMol Molecular Graphics System.

Sharma, M., Abayakoon, P., Epa, R., Jin, Y., Lingford, J.P., Shimada, T., Nakano, M., Mui, J.W.Y.W.-Y., Ishihama, A., Goddard-Borger, E.D., Davies, G.J., Williams, S.J., 2021. Molecular basis of sulfosugar selectivity in sulfoglycolysis. ACS Cent. Sci. 7, 476–487. https://doi.org/10.1021/acscentsci.0c01285.

Sharma, M., Abayakoon, P., Lingford, J.P., Epa, R., John, A., Jin, Y., Goddard-Borger, E.D., Davies, G.J., Williams, S.J., Epa, R., Goddard-Borger, E.D., Davies, G.J., Williams, S.J., 2020. Dynamic structural changes accompany production of Dihydroxypropanesulfonate by Sulfolactaldehyde reductase. ACS Catal. 10, 2826–2836. https://doi.org/10.26434/chemrxiv.9725120.v2.

Sharma, M., Lingford, J.P., Petricevic, M., Snow, A.J.D., Zhang, Y., Järvå, M.A., Mui, J.W.-Y., Scott, N.E., Saunders, E.C., Mao, R., Epa, R., Silva, B.M. da, Pires, D.E.V., Ascher, D.B., McConville, M.J., Davies, G.J., Williams, S.J., Goddard-Borger, E.D., 2022. Oxidative desulfurization pathway for complete catabolism of sulfoquinovose by bacteria. Proc. Natl. Acad. Sci. Unit. States Am. 119, e2116022119. https://doi.org/10.2185/jjrm.23.202.

Shlykov, M.A., Zheng, W.H., Chen, J.S., Saier, M.H., 2012. Bioinformatic characterization of the 4-Toluene Sulfonate Uptake Permease (TSUP) family of transmembrane proteins. Biochim. Biophys. Acta Biomembr. 1818, 703–717. https://doi.org/10.1016/j.bbamem.2011.12.005.

Snow, A.J.D., Burchill, L., Sharma, M., Davies, G.J., Williams, S.J., 2021. Sulfoglycolysis: catabolic pathways for metabolism of sulfoquinovose. Chem. Soc. Rev. 50, 13628–13645.

Speciale, G., Jin, Y., Davies, G.J., Williams, S.J., Goddard-Borger, E.D., 2016. YihQ is a sulfoquinovosidase that cleaves sulfoquinovosyl diacylglyceride sulfolipids. Nat. Chem. Biol. 12, 215–217. https://doi.org/10.1038/nchembio.2023.

Spurlino, J.C., Lu, G.Y., Quiocho, F.A., 1991. The 2.3-A resolution structure of the maltose- or maltodextrin-binding protein, a primary receptor of bacterial active transport and chemotaxis. J. Biol. Chem. 266, 5202–5219. https://doi.org/10.1016/s0021-9258(19)67774-4.

Tang, C., Schwieters, C.D., Clore, G.M., 2007. Open-to-closed transition in apo maltose-binding protein observed by paramagnetic NMR. Nature 449, 1078–1082. https://doi.org/10.1038/nature06232.

Thomas, C., Tampé, R., 2020. Structural and mechanistic principles of ABC transporters. Annu. Rev. Biochem. 89, 605–636. https://doi.org/10.1146/annurev-biochem-011520-105201.

Tian, W., Chen, C., Lei, X., Zhao, J., Liang, J., 2018. CASTp 3.0: computed atlas of surface topography of proteins. Nucleic Acids Res. 46, W363–W367. https://doi.org/10.1093/nar/gky473.

Tófoli De Araújo, F., Bolanos-Garcia, V.M., Pereira, C.T., Sanches, M., Oshiro, E.E., Ferreira, R.C.C., Chigardze, D.Y., Gonçalves Barbosa, J.A., Ferreira, L.C.D.S., Benedetti, C.E., Blundell, T.L., Balan, A., 2013. Structural and physiological analyses of the alkanesulphonate-binding protein (SsuA) of the citrus pathogen Xanthomonas citri. PLoS One 8, e80083. https://doi.org/10.1371/journal.pone.0080083.

Vagin, A., Teplyakov, A., 2010. Molecular replacement with MOLREP. Acta Crystallogr. Sect. D Biol. Crystallogr. 66 (1), 22–25. https://doi.org/10.1107/S0907444909042589.

Winter, G., 2010. Xia2: an expert system for macromolecular crystallography data reduction. J. Appl. Crystallogr. 43 (1), 186–190. https://doi.org/10.1107/S0021889809045701.

Zhang, Y., Mui, J.W.Y., Arumaperuma, T., Lingford, J.P., Goddard-Borger, E.D., White, J.M., Williams, S.J., 2020. Concise synthesis of sulfoquinovose and sulfoquinovosyl diacylglycerides, and development of a fluorogenic substrate for sulfoquinovosidases. Org. Biomol. Chem. 18, 675–686. https://doi.org/10.1039/c9ob02540e.